

Measurement of the angular correlation between the two gamma rays emitted in the radioactive decays of a ^{60}Co source with two NaI(Tl) scintillators

E. C. Amato¹, A. Anelli¹, M. Barbieri¹, D. Cataldi¹,
 V. Cellamare¹, D. Cerasole¹, F. Conserva¹, S. De Gaetano^{1,2},
 D. Depalo¹, A. Digennaro¹, E. Fiorente¹, F. Gargano²,
 D. Gatti¹, P. Loizzo¹, F. Loparco^{1,2,*}, O. Mele¹, N. Nicassio¹,
 G. Perfetto¹, R. Pillera^{1,2}, R. Pirlo¹, E. Schygulla¹, D. Troiano¹

¹ Dipartimento di Fisica “M. Merlin” dell’Università e del Politecnico di Bari, I-70126 Bari, Italy

² Istituto Nazionale di Fisica Nucleare, Sezione di Bari, 70126 Bari, Italy

E-mail: francesco.loparco@ba.infn.it

Abstract. We implemented a didactic experiment to study the angular correlation between the two gamma rays emitted in typical ^{60}Co radioactive decays. We used two NaI(Tl) scintillators, already available in our laboratory, and a low-activity ^{60}Co source. The detectors were mounted on two rails, with the source at their center. The first rail was fixed, while the second could be rotated around the source. We performed several measurements by changing the angle between the two scintillators in the range from 90° to 180° . Dedicated background runs were also performed, removing the source from the experimental setup. We found that the signal rate increases with the angular separation between the two scintillators, with small discrepancies from the theoretical expectations.

1. Introduction

Cobalt-60 (^{60}Co) is among the radioactive isotopes of cobalt with a spin-parity $J^P = 5^+$ and undergoes beta decay with a half-life of 1925.20 ± 0.25 days [1, 2]. A 99.88% fraction of the beta decays [3] leads to an excited state of ^{60}Ni with a spin-parity $J^P = 4^+$, which subsequently decays, passing through the intermediate state $J^P = 2^+$, into the ground state $J^P = 0^+$ with the emission of two gamma rays, respectively with energies of 1.17 MeV and 1.33 MeV. Since the lifetime of the intermediate state is of the order of 10^{-12} s [4] and is much smaller than typical experimental time resolutions, the two gamma rays are expected to be detected in coincidence.

General considerations of radiation theory show that the emission directions of consecutive gamma rays produced by an excited nucleus are correlated [5]. These transitions involve three nuclear states and the multipole order of the emitted radiation

determines the angular separations between the two photons. The angular correlation can be described in terms of the relative probability per unit solid angle $W(\theta)$ of the second photon to be emitted at an angle θ with respect to the first one. Explicit quantum mechanical calculations by Hamilton show that, apart from a constant factor, the correlation function has the general form:

$$W(\theta) = 1 + \sum_{k=1}^L \alpha_k (\cos \theta)^{2k} \quad (1)$$

where L is the lowest angular momentum of the two gamma rays. Calculations by Hamilton provide the theoretical values of the coefficients α_k in case of dipole and quadrupole radiation for all possible nuclear angular momenta. In the case of ^{60}Co , both transitions can be assumed to be electric quadrupoles, and the angular correlation function is given by:

$$W(\theta) = 1 + \frac{1}{8} \cos^2 \theta + \frac{1}{24} \cos^4 \theta \quad (2)$$

Several measurements of the angular correlations between the photons produced in the ^{60}Co decays were performed in the past and the experimental results were found in agreement with the predictions from Hamilton's model (see for instance refs. [4, 6, 7, 8, 9]). We have designed and implemented a custom experimental setup to perform this measurement in a didactic laboratory for undergraduate Physics students with the instrumentation already available.

2. Experimental setup

A photo of the experimental setup is shown in Fig. 1. The ^{60}Co source is a 1 mm thick disk with a diameter of 1 cm and an activity of ~ 5 kBq placed on a holder mounted at the center of a table. The detectors are two cylindrical NaI(Tl) scintillators coupled with photomultiplier tubes (PMTs), which can be moved along two rails placed on the table. The first scintillator (S_0 hereafter), which has a diameter of 8.2 cm and a height of 8.2 cm, is mounted on a fixed rail. The second scintillator (S_1 hereafter), which has a diameter of 5.8 cm and a height of 5.8 cm, is mounted on a mobile rail, which can be rotated around the source with respect to the fixed one. A graduated scale, divided in sections of 5° step between 0° and 180° , is drawn on the table and is used to measure the angle between the two rails. Both scintillators can be also moved along the rails at different distances from the source.

During our measurements, the scintillators S_0 and S_1 were placed at distances of 20 cm and of 14.1 cm from the source, respectively. In this way, the solid angle subtended by each scintillator with respect to the source was $\Delta\Omega \simeq 0.132$ sr. This geometry provided a good compromise between the need of taking data with a high enough rate and the need of keeping a limited uncertainty on the angle between the two scintillators. Indeed, the latter is determined by the radius of the two scintillators and by their distances from the source and it amounts to $\Delta\theta \sim 16^\circ$.

The signals from the two scintillators were acquired using a digital oscilloscope *Teledyne Le Croy WaveRunner 6 Zi* [10]. Fig. 2 shows a scheme of the trigger logic. The analog signals from the PMTs coupled with S_0 and S_1 are sent to two linear fan-in/fan-out modules, producing two copies of each input signal. A copy of the two signals from S_0 and S_1 is sent to the oscilloscope (channels 1 and 2 in the scheme of Fig. 2). The second copy is sent to a discriminator module with a threshold set at -30 mV. The logic signals from the discriminator are sent to a logic unit, where the trigger to the oscilloscope is formed (channel 3 in the scheme of Fig. 2).

The logic unit allows the implementation of different trigger configurations. We performed our measurements with the following ones:

- “and” configuration: in this case we required both signals from S_0 and S_1 with pulse height exceeding the threshold. This configuration was implemented to select events with a gamma-ray in each scintillator;
- “or” configuration: in this case we required a signal above the threshold from either S_0 or S_1 . This configuration was implemented to perform energy calibrations, as discussed in Sec. 3;

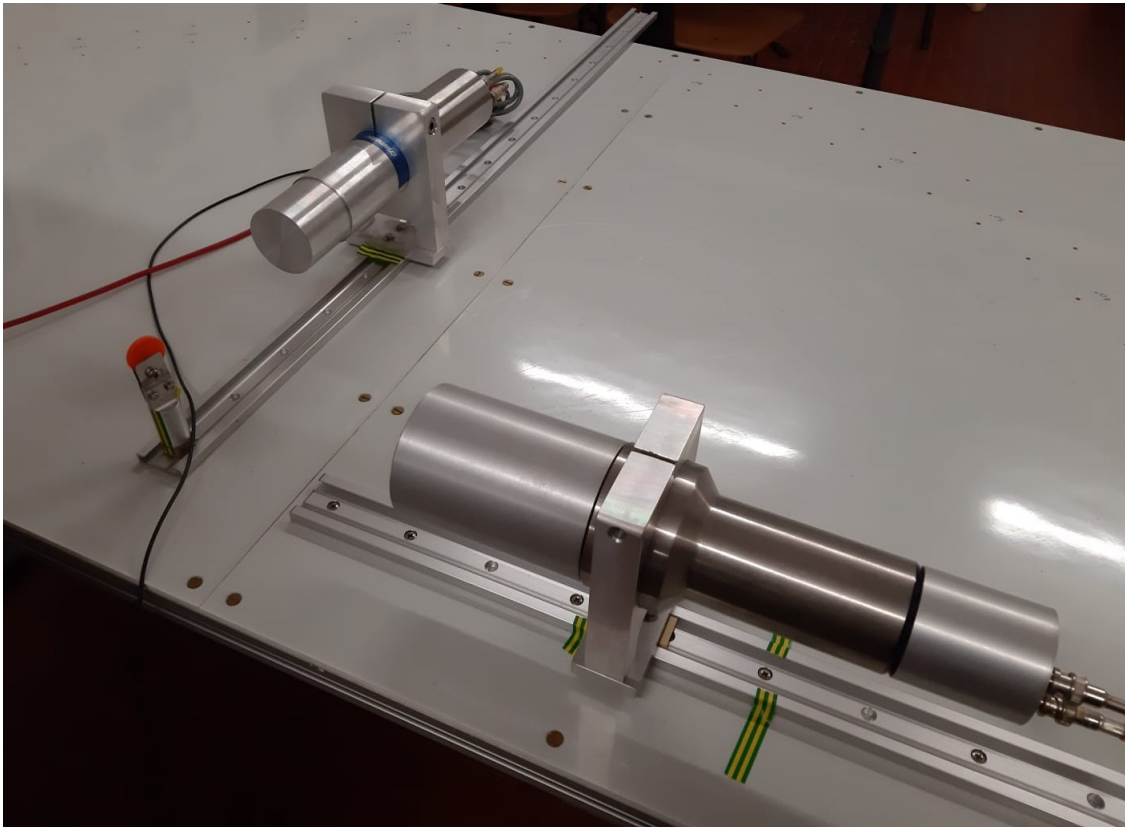


Figure 1. Photo of the experimental setup. The scintillator S_0 is mounted on the fixed rail on the right, while the scintillator S_1 is mounted on the mobile rail on the left. The ^{60}Co source is the orange disk placed in the holder shown at the center of the picture.

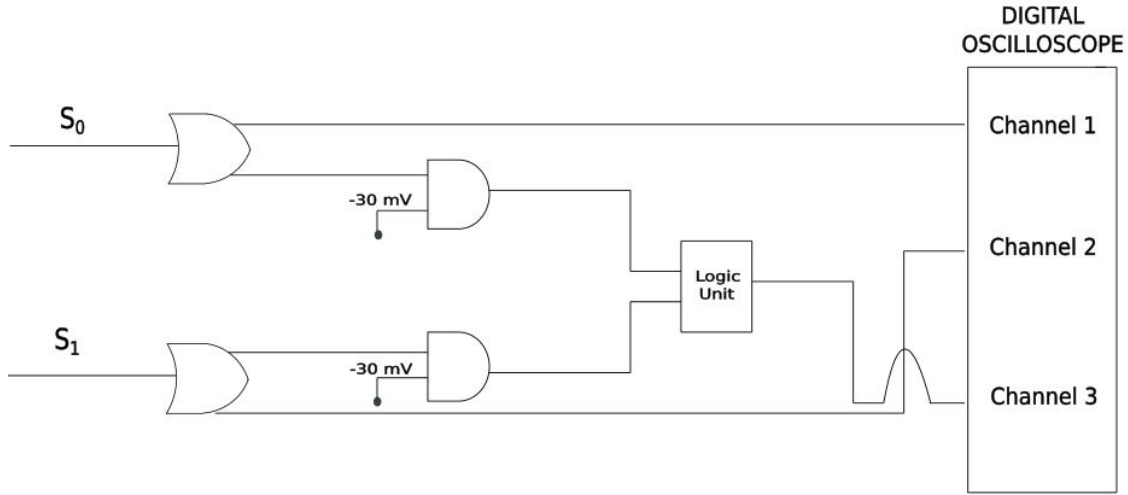


Figure 2. Schematic of the trigger logic. The analog signals from S_0 and S_1 are sent to two fan-in/fan-out modules. Each module provides two copies of the corresponding input signal. A copy of the two signals is sent to the oscilloscope, while the other one is sent to a discriminator with a threshold fixed at -30 mV . The logic output signals from the discriminators are sent to a logic unit, which provides the trigger signal to the oscilloscope.

- “single scintillator” configuration: in this case we required a signal above the threshold only from S_0 (or S_1). This configuration was also implemented to perform energy calibrations.

Fig. 3 shows an example of the analog signals from the two scintillators recorded when the trigger logic was set in the “and” configuration with the ^{60}Co source. The signals are likely originated by two gamma rays from the source being absorbed in the two scintillators. We see that both signals exhibit a rise time of a few tens of ns and a fall time of a few hundreds of ns. These values are expected, since the decay time of the fluorescence light in NaI(Tl) scintillators is of 230 ns [11] and the time constant RC of the readout circuit is $\simeq 15\text{ ns}$ (this value is obtained from the oscilloscope input resistance $R = 50\ \Omega$ and from the cable capacitance of about 300 pF).

We used the oscilloscope to measure the amplitudes of the pulses from both scintillators and the integral of each pulse in a $1\ \mu\text{s}$ time window. This information is important since the value of the time integral is proportional to the charge released in each scintillator. We also measured the time intervals between events. The data taken were stored in ROOT files [12], which are easily accessible for data analysis.

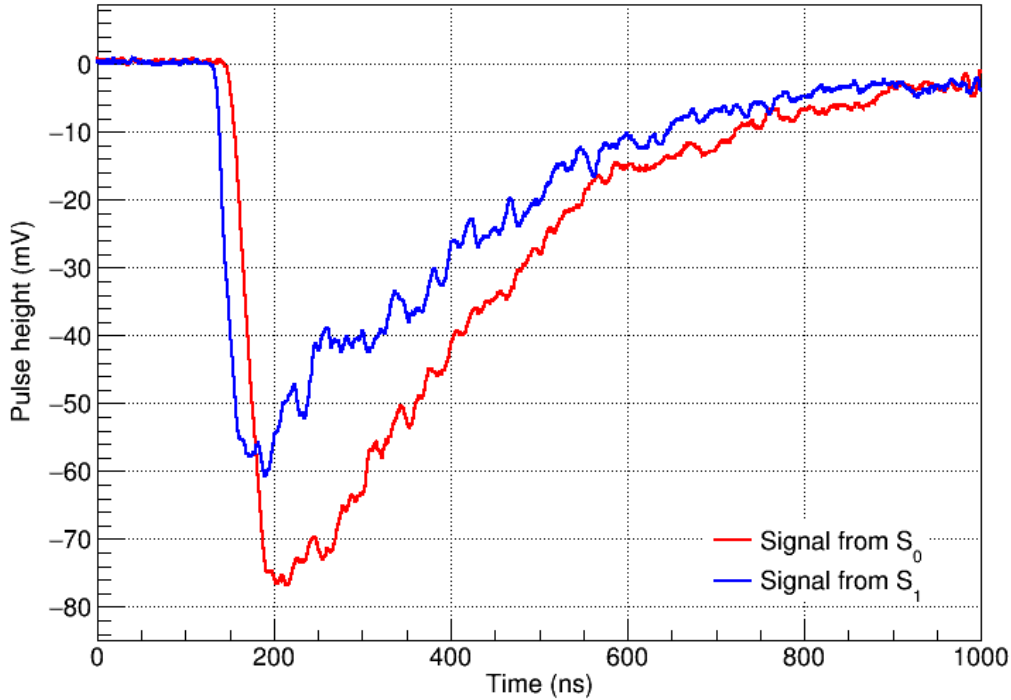


Figure 3. Example of the analog signals produced in the two scintillators by the gamma rays emitted from the ^{60}Co source.

3. Energy calibration

We performed the energy calibration of the two scintillators with the ^{60}Co source and with a ^{137}Cs source. The ^{60}Co source is used to calibrate the detectors with 1.17 MeV and 1.33 MeV photons. Moreover, if both photons are detected in the same scintillator, an additional calibration point corresponding to the sum of the energies of the two photons (2.50 MeV) is available. The ^{137}Cs source emits a gamma-ray of 0.662 MeV [3] and provides a calibration point at low energies.

Fig. 4 shows the charge distributions obtained when taking data in the “single scintillator” trigger configuration with the ^{60}Co and ^{137}Cs sources. The full-energy peaks in the two scintillators were fitted with gaussian functions. The charge values of each peak were evaluated as the mean values of the corresponding fit function.

A further calibration point is provided by the position of the “pedestal” peak, which corresponds to a null energy deposition in the scintillator. The position of the pedestal peak in each scintillator was evaluated from its charge distribution in a run with the ^{137}Cs source in the “single scintillator” trigger configuration, in which the trigger was provided by the other one.

The results of the energy calibrations are summarized in Fig. 5. The data of both scintillators are well fitted with straight lines. We see that the charge depends linearly

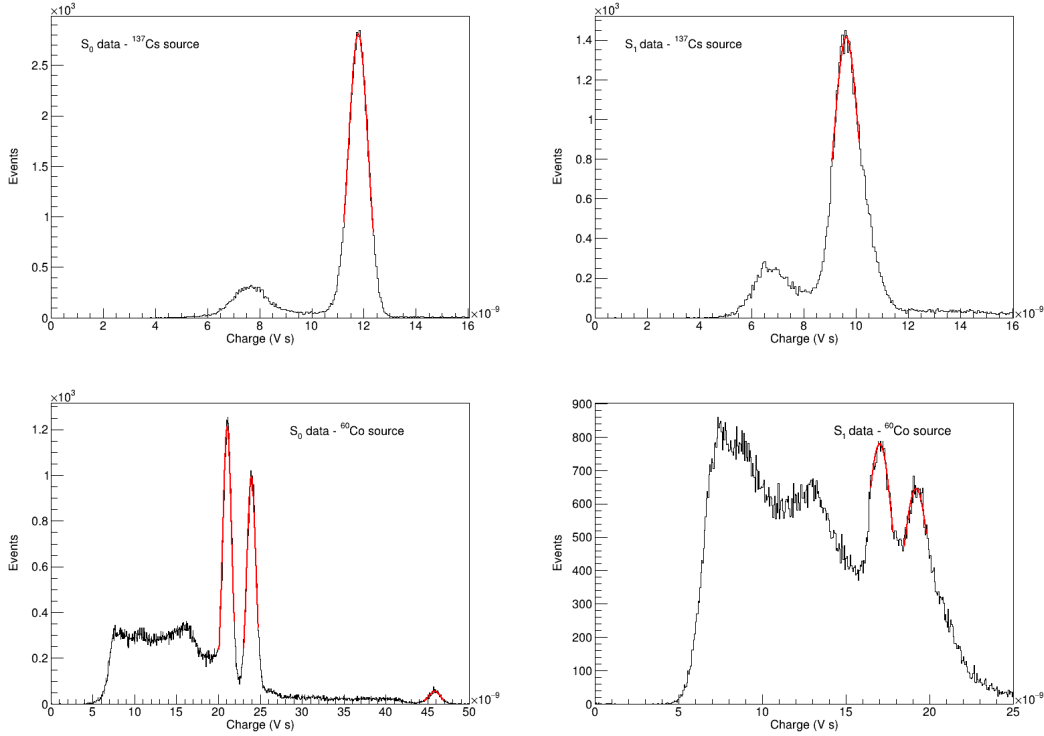


Figure 4. Charge distributions obtained with the ^{137}Cs source (top row) and with the ^{60}Co source (bottom row). The plots on left column refer to the scintillator S_0 , while those on the right column refer to the scintillator S_1 . All data have been taken in the “single scintillator” trigger configuration. The full-energy peaks have been fitted with gaussian functions and the fits are indicated with red lines. In the case of ^{60}Co source, the full-energy peak corresponding to the sum of the energies of the two photons in the scintillator S_1 was not clearly visible and was therefore not fitted.

on the energy deposited in the scintillators in the range of interest for our measurements.

Finally, we studied the behaviour of the energy resolution σ_E/E as a function of the energy deposited in the scintillators. The energy resolution was evaluated from the fits of the full-energy peaks of the ^{60}Co and ^{137}Cs spectra used to perform the energy calibrations. The results are shown in Fig. 6. We see that the energy resolution for the ^{60}Co gamma rays is about 2.5% for S_0 and about 5% for S_1 .

We also fitted our data with functions which are commonly used in high-energy physics to describe the energy resolution of electromagnetic calorimeters [13]. In particular, the data of S_0 have been fitted with the function:

$$\frac{\sigma_E}{E} = \frac{a}{\sqrt{E(\text{MeV})}} \quad (3)$$

where $a = (2.464 \pm 0.006) \times 10^{-2}$, while the data of S_1 have been fitted with the function:

$$\frac{\sigma_E}{E} = \frac{a}{\sqrt{E(\text{MeV})}} \oplus b \quad (4)$$

where the \oplus symbol indicates the sum in quadrature, $a = (2.508 \pm 0.181) \times 10^{-2}$ and

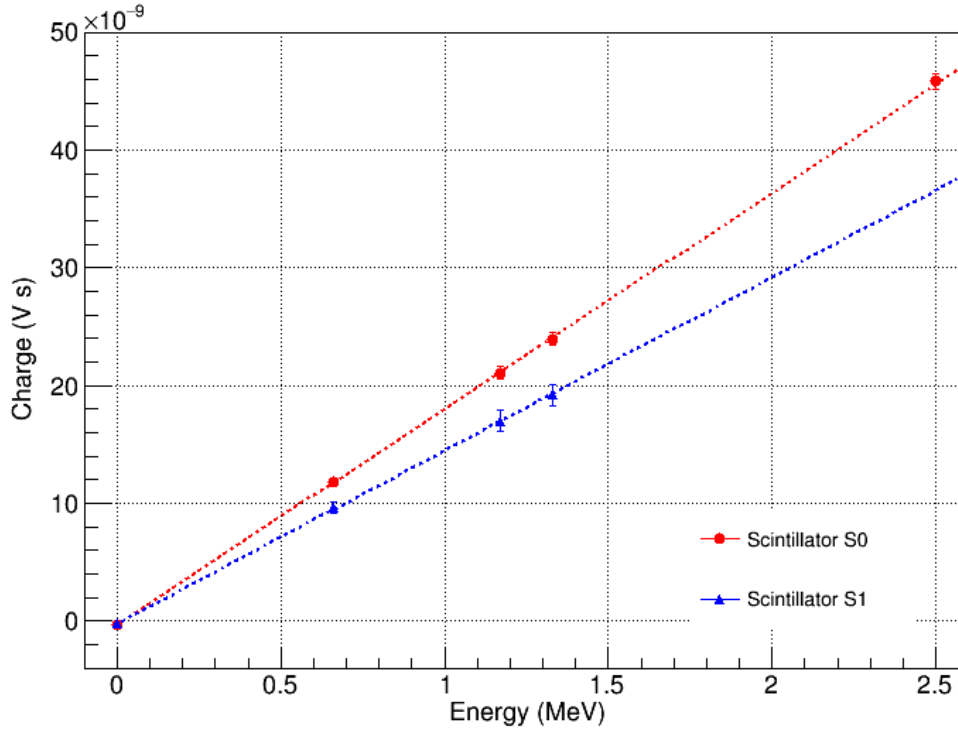


Figure 5. Energy calibration of the two scintillators. The markers indicate the charges corresponding to the mean values of the gaussian functions fitting the peaks of the spectra obtained in the calibration runs. The data have been fitted with straight lines, which are also shown in the plot.

$b = (4.254 \pm 0.095) \times 10^{-2}$. We see that the resolution of S_0 is mainly dominated by the stochastic term, while in the case of S_1 the constant term cannot be neglected.

4. Event selection and data analysis

To measure the angular correlations between the gamma rays emitted in the ^{60}Co decays we performed several runs in the “and” trigger configuration, changing the angle between the two detectors. Two sets of measurements were performed for each angle. The first measurement was performed with the ^{60}Co source placed on its holder, while the second was performed removing the source from the experimental setup. The second set of measurements was needed to evaluate the background rates due to natural radioactivity and cosmic rays penetrating in our laboratory.

Figs. 7 and 8 show a summary of the data taken by the two scintillators in the runs with the ^{60}Co source. In Fig. 7 we show the average rate of events as a function of the energies E_0 and E_1 measured by the two detectors. The following regions can be identified in the plot:

- the two peaks at the positions (1.17 MeV, 1.33 MeV) and (1.33 MeV, 1.17 MeV)

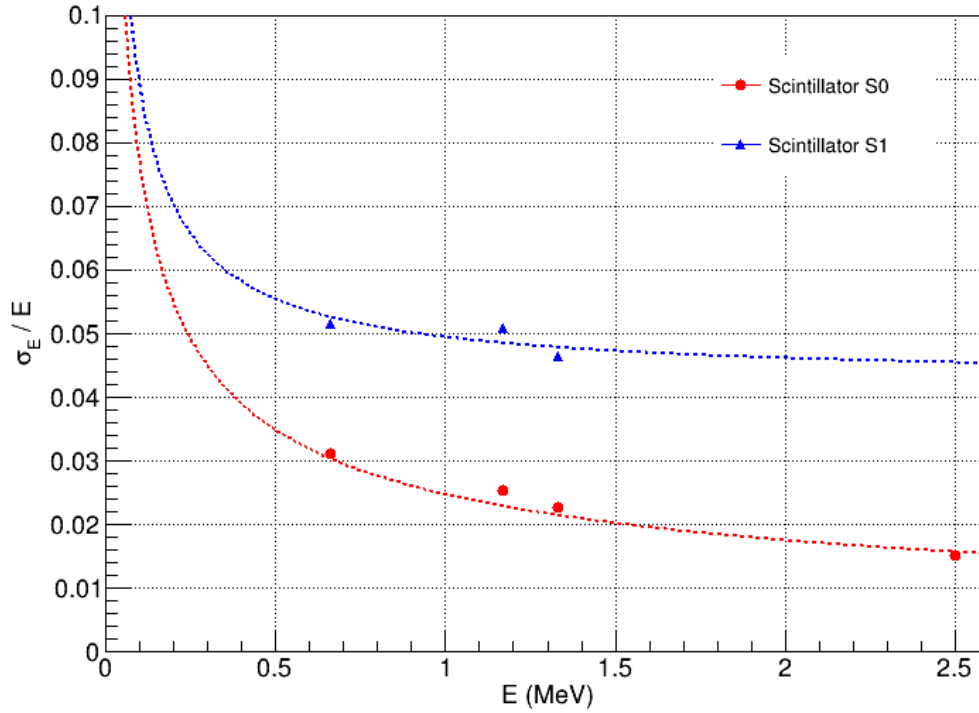


Figure 6. Energy resolution as a function of the energy deposited in the scintillators. The data of S_0 and S_1 have been fitted with the functions in Eqs. 3 and 4, respectively. The best fit curves are represented by the dashed lines.

correspond to events where one of the two photons from the ^{60}Co decay is absorbed in S_0 and the second one is absorbed in S_1 , with both gamma rays depositing their whole energy in the scintillator in which they are absorbed. In these events both gamma rays have likely undergone a photoelectric interaction with the scintillator material and the resulting photoelectron has been absorbed in the scintillator;

- the vertical bands below the peaks correspond to events where the photon absorbed in S_0 releases its whole energy in the scintillator, while the photon absorbed in S_1 releases only a fraction of its energy in the scintillator. In this case the second photon has likely undergone a Compton scattering, with the electron being absorbed in the scintillator and the scattered photon escaping from the detector;
- the horizontal bands on the left side of the peaks can be interpreted in a similar way as in the previous case, with the inversion of the roles of S_0 and S_1 . The rate of these events is smaller than that in the previous region due to the smaller size of S_1 with respect to S_0 ;
- the diagonal bands centered on the lines $E_0 + E_1 = 1.17\text{MeV}$ and $E_0 + E_1 = 1.33\text{MeV}$ correspond to events where one of the two photons undergoes Compton scattering in a scintillator, with the scattered photon being absorbed in the other scintillator;

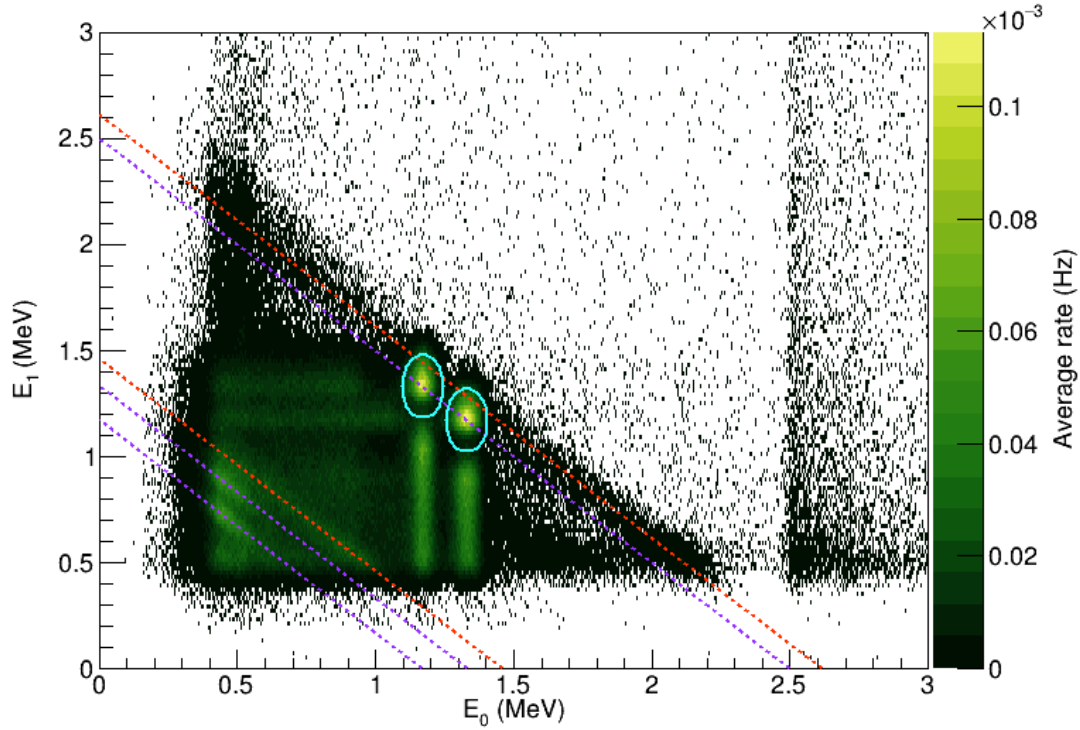


Figure 7. Average rate of events as a function of the energy deposited in the two scintillators in the runs with the ^{60}Co source. The violet dashed lines correspond to the energies of the two photons emitted by the ^{60}Co source (1.17 MeV and 1.33 MeV) and to the sum of the energies of both photons (2.50 MeV). The orange dashed lines correspond to the energies of photons produced in the decays of ^{40}K and ^{208}Tl (1.461 MeV and 2.610 MeV, respectively). The cyan continuous lines indicate the ellipses used for the event selection.

- the diagonal band centered on the line $E_0 + E_1 = 2.50$ MeV corresponds to events where the first photon is absorbed in one of the two scintillators, the second photon undergoes Compton scattering in the same scintillator and the scattered photon is absorbed in the other scintillator;
- the diagonal bands centered on the lines $E_0 + E_1 = 1.46$ MeV and $E_0 + E_1 = 2.61$ MeV correspond to events where a gamma-ray from the decay of ^{40}K or ^{208}Tl undergoes Compton scattering in a scintillator with the scattered photon being absorbed in the other scintillator. These decays mostly originate from the ^{40}K in the glass windows of the PMTs and from the ^{208}Tl in the scintillators.
- the region $E_0 > 2.5$ MeV which is populated by events where either both the photons from the ^{60}Co decays or the gamma-ray from the ^{208}Tl decay are fully absorbed in S_0 , in coincidence with a cosmic-ray event in S_1 .

The same features can be observed also in Fig. 8, which shows the average rates as a function of the energies E_0 and E_1 and of their sum. Looking at the energy spectra

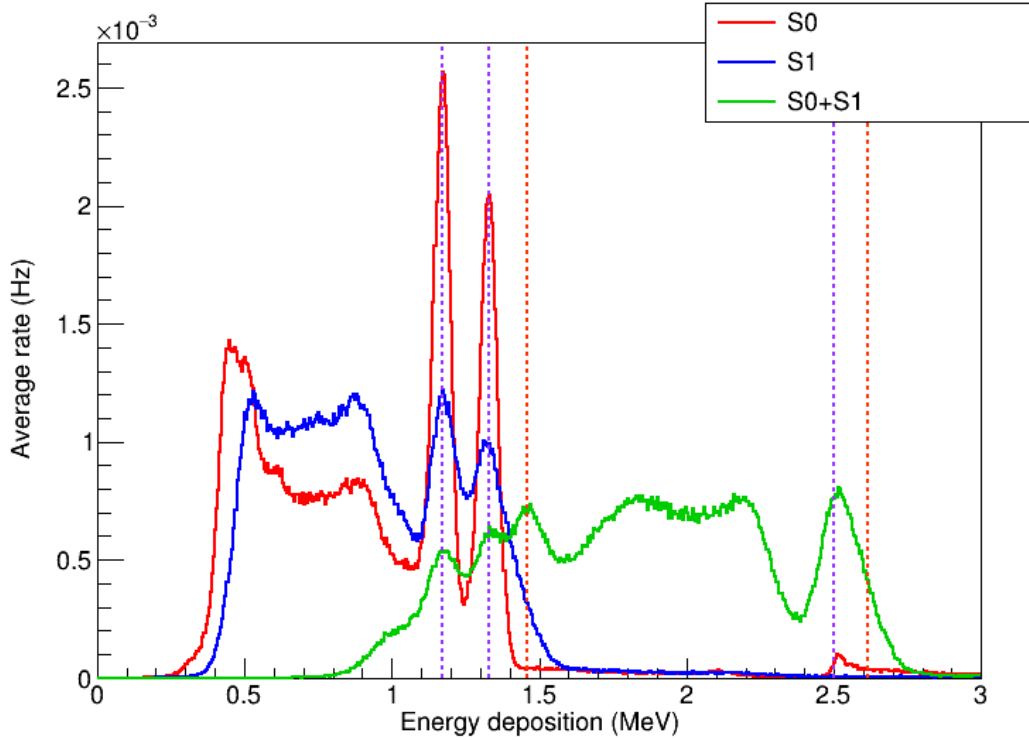


Figure 8. Average rate of events as a function of the energy deposited in each of the two scintillators in the runs with the ^{60}Co source. The violet dashed lines correspond to the energies of the two photons emitted by the ^{60}Co source (1.17 MeV and 1.33 MeV) and to the sum of the energies of both photons (2.50 MeV). The orange dashed lines correspond to the energies of photons produced in the decays of ^{40}K and ^{208}Tl (1.461 MeV and 2.610 MeV, respectively).

in S_0 and S_1 we see that, as expected, the Compton shoulder in S_1 is more relevant than in S_0 , due to its smaller size. Looking at the distribution of total energy deposited in the scintillators we also see that the rate of events in the peak corresponding to the ^{40}K line is similar to that of events in the peak corresponding to the detection of both gamma rays from ^{60}Co .

Figs. 9 and 10 show the distributions of energy depositions in the two scintillators obtained in the runs without the ^{60}Co source. Comparing Fig. 9 with Fig. 7, we see a significant rate drop in the regions corresponding to events from ^{60}Co . The diagonal bands corresponding to photons from ^{40}K and ^{208}Tl decays become more evident, and additional diagonal bands corresponding to photons produced in the decays of other radioactive isotopes are also visible. Looking at the shape of individual energy spectra of S_0 and S_1 shown in Fig. 10, we see that they are dominated by cosmic-ray events, with a contribution from natural radioactivity. This contribution becomes more evident when looking at the distribution of the total energy deposited in the two scintillators.

A further comparison between the data taken in the runs with and without the ^{60}Co source is shown in Fig. 11, where the energy spectra in the two scintillators are

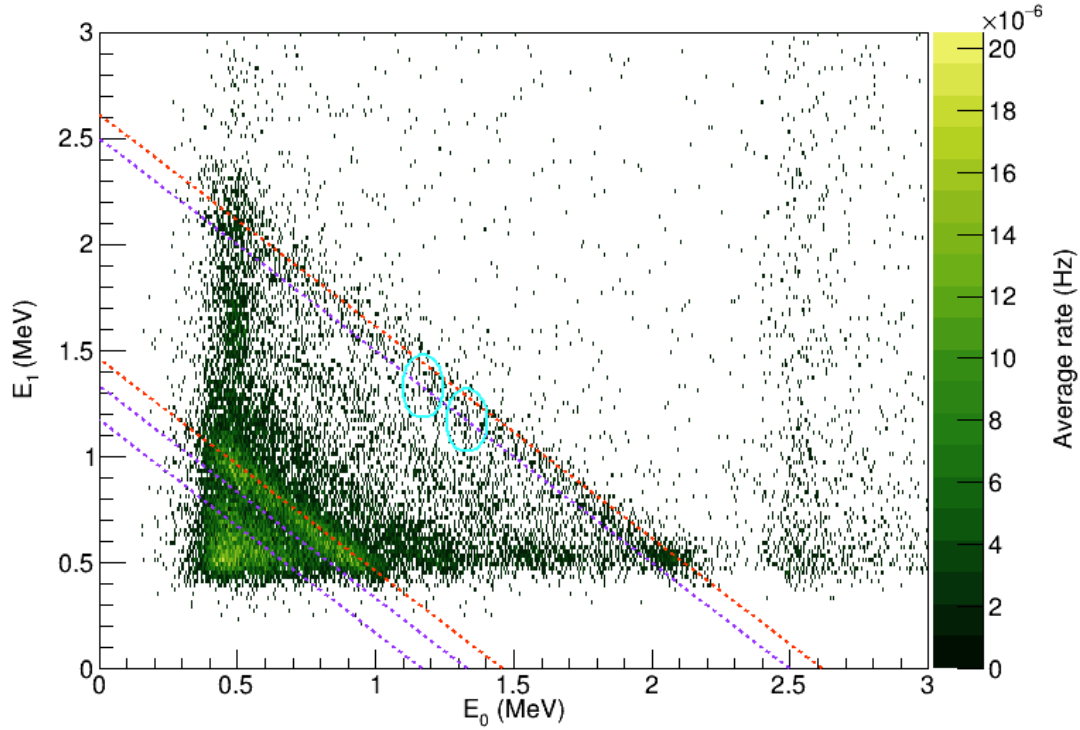


Figure 9. Average rate of events as a function of the energy deposited in the two scintillators in the runs without the ^{60}Co source. The lines have the same meanings as in Fig.7.

represented. We see that, for energy depositions above 1.33 MeV in both scintillators, the rate of events with the ^{60}Co source is consistent with the rate of events without the source.

In our analysis we selected events in the regions corresponding to the two peaks shown in Fig. 7. The selection was performed discarding events outside the ellipses defined by the following equations:

$$\frac{(E_0 - 1.17 \text{ MeV})^2}{a^2} + \frac{(E_1 - 1.33 \text{ MeV})^2}{b^2} = 1 \quad (5)$$

$$\frac{(E_0 - 1.33 \text{ MeV})^2}{a^2} + \frac{(E_1 - 1.17 \text{ MeV})^2}{b^2} = 1 \quad (6)$$

where $a = 0.075 \text{ MeV}$ and $b = 0.150 \text{ MeV}$. We set the values of a and b to about 3 times the energy resolutions of S_0 and S_1 at 1 MeV. The contours of the ellipses in Eqs. 5 and 6 are shown in the plots of Figs. 7 and 9.

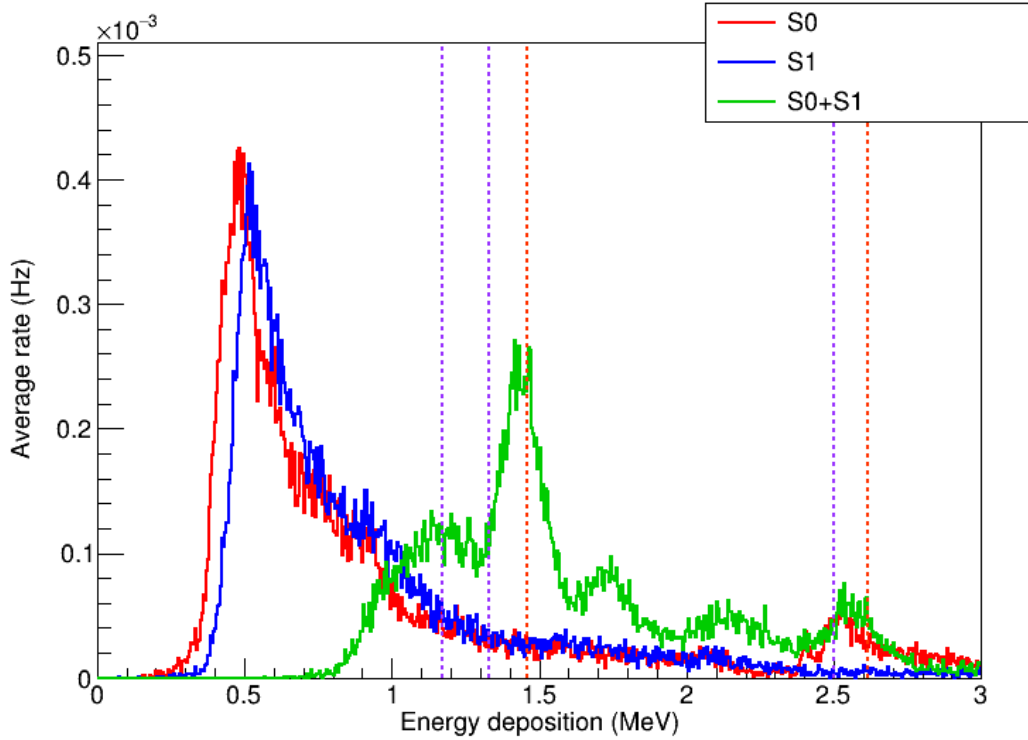


Figure 10. Average rate of events as a function of the energy deposited in each of the two scintillators in the runs without the ^{60}Co source. The lines have the same meanings as in Fig. 8.

5. Results and discussion

We performed several measurements, changing the opening angle between the two scintillators in the range between 90° and 180° with 15° steps. The event selection illustrated in Sec. 4 was applied to the runs taken in the different configurations explored. The signal rate at each angle was evaluated as the difference between the rate of selected events with the ^{60}Co source and the rate of selected events without the source. Our results are summarized in Fig. 12.

We have fitted the experimental data with the function:

$$r(\theta) = r_0 (1 + a \cos^2 \theta + b \cos^4 \theta) \quad (7)$$

where r_0 corresponds to the rate when the angle between the two scintillators is 90° and the expected values of the parameters a and b , according to Hamilton's theoretical model, are 0.125 and 0.042 respectively. In our fit we find the values $r_0 = (2.303 \pm 0.021) \times 10^{-2}$ Hz, $a = 0.249 \pm 0.058$ and $b = (-6.43 \pm 5.88) \times 10^{-2}$ with a $\chi^2/d.o.f. = 0.77/4$.

As expected, we find that the signal rate increases when increasing the opening angle between the two scintillators. However, our results slightly deviate from Hamilton's model predictions. In particular, we find a discrepancy of about 2σ on both the

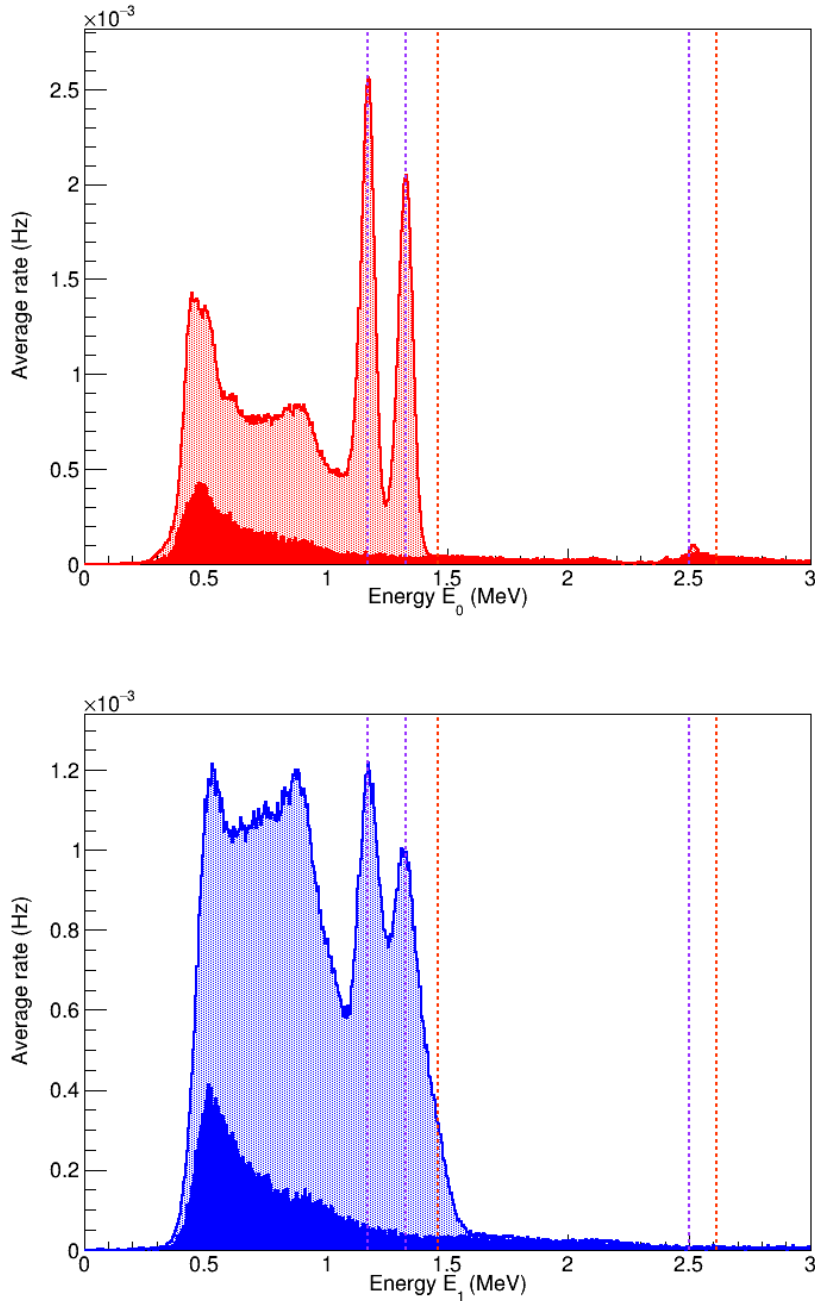


Figure 11. Average rate of events as a function of the energy deposited in S_0 (top panel) and S_1 (bottom panel). The data collected in the runs with the ^{60}Co source (histograms with shaded areas) are compared with those collected in the runs without the source (histograms with filled area). The lines have the same meanings as in Fig. 8.

parameters a and b with respect to their theoretical values. These discrepancies can be due to several reasons. In our setup we used a low-activity source and we had to place the scintillators very close to the source to keep a sufficiently high event rate during data taking. As discussed in Sec. 2, this configuration implies an uncertainty on the

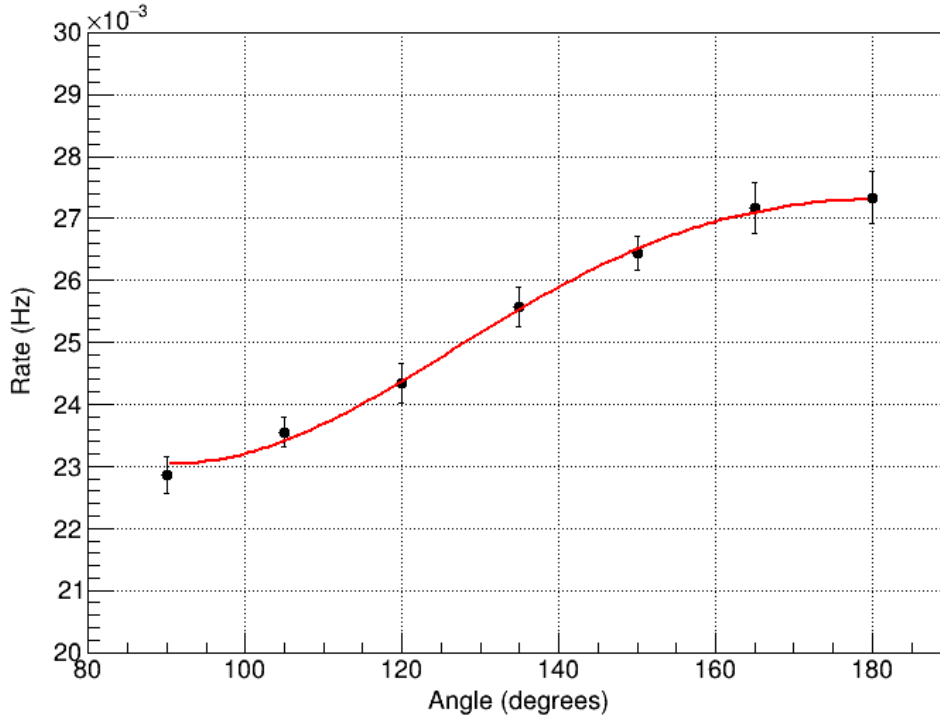


Figure 12. Average rate of signal events as a function of the opening angle between S_0 and S_1 . The red line represents the fit function.

opening angle which, on the basis only of pure geometrical considerations, is of about 16° . Placing the scintillators at larger distances from the source would allow the minimization of this uncertainty. Another possible cause could be the finite size of the ^{60}Co source used in our measurement. In Hamilton's model it is assumed that the radioactive source is pointlike. However, as discussed in Sec. 2, our source was encapsulated in a disk of 1 cm diameter and 1 mm thickness. When the mobile scintillator was rotated at different angles (see Fig. 1), the source was always kept in the same position, and therefore its projected cross section on the front area of the mobile scintillator changed with the rotation angle.

The measurement illustrated in this work can be improved in several ways. First of all, one could use two large size scintillators (i.e. at least with the size of S_0 in our setup) to enhance the probability that both gamma rays deposit their whole energy within the scintillator volumes. A further enhancement could be also obtained using a source with a higher activity, which would allow the scintillators to be placed at larger distances, thus improving the precision in the angle definition. Finally, the effects of possible asymmetries in the shape of the source could be minimized using a rotating source.

References

- [1] M. P. Unterweger, D. D. Hoppes, and F. J. Schima. New and revised half-life measurements results. *Nuclear Instruments and Methods in Physics Research A*, 312(1):349–352, February 1992.
- [2] M. P. Unterweger. Half-life measurements at the National Institute of Standards and Technology. *Applied Radiation and Isotopes*, 56(1-2):125–130, Jan-Feb 2002. Conference on Radionuclide Metrology and Its Application (ICRM 2001), May 14-18, 2001.
- [3] Data taken from the Laboratoire National Henri Bequerel online database. <http://www.lnhb.fr/nuclear-data/module-lara/>. Accessed: 2021-12-01.
- [4] E. L. Brady and M. Deutsch. Angular correlation of successive gamma-rays. *Phys. Rev.*, 78:558–566, Jun 1950.
- [5] D. R. Hamilton. On Directional Correlation of Successive Quanta. *Phys. Rev.*, 58:122–131, 1940.
- [6] Wilfred M. Good. The Angular Distribution of Gamma-Rays in Na^{24} , Co^{60} , Y^{88} . *Phys. Rev.*, 70:978–979, Dec 1946.
- [7] Rossi A. Colombo, S. and A. Scotti. A precision re-measurement of the ^{60}Ni gamma-gamma directional correlation function. *Il Nuovo Cimento*, 2:471–486, 1955.
- [8] J. K. Smith, A. D. MacLean, W. Ashfield, A. Chester, A. B. Garnsworthy, and C. E. Svensson. Gamma–gamma angular correlation analysis techniques with the GRIFFIN spectrometer. *Nucl. Instrum. Meth. A*, 922:47–63, 2019.
- [9] E. D. Klema and F. K. McGowan. Gamma-Gamma Angular Correlation in Ni^{60} . *Phys. Rev.*, 91:616–618, Aug 1953.
- [10] WaveRunner 6 Zi and HRO Operator’s Manual. <https://cdn.teledynelecroy.com/files/manuals/waverunner-6zi-operators-manual.pdf>. Accessed: 2021-10-01.
- [11] Glenn F Knoll. *Radiation detection and measurement*. John Wiley & Sons, 2010.
- [12] R. Brun and F. Rademakers. ROOT: An object oriented data analysis framework. *Nucl. Instrum. Meth. A*, 389:81–86, 1997.
- [13] P.A. Zyla et al. Review of Particle Physics. *PTEP*, 2020(8):083C01, 2020.